Degenerate polygonal tilings in simple animal tissues

A. Hočevar[1] and P. Ziherl[1,2]
[1]*Department of Theoretical Physics, J. Stefan Institute, Jamova 39, SI-1000 Ljubljana, Slovenia*
[2]*Department of Physics, Faculty of Mathematics and Physics, University of Ljubljana, Jadranska 19, SI-1000 Ljubljana, Slovenia*
(Received 27 March 2009; published 2 July 2009)

The salient feature of one-cell-thick epithelia is their en face view, which reveals the polygonal cross section of the close-packed prismatic cells. The physical mechanisms that shape these tissues were hitherto explored using theories based on cell proliferation, which were either entirely topological or included certain morphogenetic forces. But mitosis itself may not be instrumental in molding the tissue. We show that the structure of simple epithelia can be explained by an equilibrium model where energy-degenerate polygons in an entropy-maximizing tiling are described by a single geometric parameter encoding their inflatedness. The two types of tilings found numerically—ordered and disordered—closely reproduce the patterns observed in *Drosophila, Hydra,* and *Xenopus* and they generalize earlier theoretical results. Free of a specific cell self-energy, cell-cell interaction, and cell division kinetics, our model provides an insight into the universality of living and inanimate two-dimensional cellular structures.

DOI: 10.1103/PhysRevE.80.011904 PACS number(s): 87.17.Pq, 87.17.Rt, 87.18.Hf

I. INTRODUCTION

Across many length scales, the forms of life are full of similar spatial patterns apparently produced by a rather generic set of morphogenetic processes. Although not new [1], the view that the universality of these processes may be related to the physical forces that materialize them—cell surface tension [2], cell adhesion [3], cortex contractility [4], etc.—is increasingly more appreciated [5–7]. With the progressing complexity of biomechanical theories of animal morphogenesis [3,4,8,9], we may soon face the question of identifying their key ingredients. In fact, this issue has already arisen in simple epithelia whose structure has been interpreted in terms of models of cell proliferation with mitotic dynamics that are either purely topological [10] or include cell elasticity and junctional forces [11]. The broader range of structures predicted by the latter more elaborate theory suggests that cell division itself may be subdominant, which reopens the problem of the origin of epithelial geometry.

The epithelium is a layered lining of organs and body cavities. The structure of its simplest one-cell-thick variant is described by the en face view showing the bases of the prismatic cells, which look like a polygonal tiling of a plane [Fig. 1(a)] [11–14]. In some cases the tiling is ordered, consisting predominantly of hexagons [12], and in others it is disordered and includes a distribution of polygon classes [13]. Either way, the structure of epithelia is essential for their function. In the *Drosophila* wing epithelium, it underlies the hexagonal packing of hairs, which direct the airflow [15]; however, the proliferating epithelium is disordered until the final stages of its growth when it transforms into the ordered pattern [12]. On the other hand, the *Drosophila* germband epithelium experiences the transition without cell division and in the opposite direction, which is instrumental for its elongation and the ensuing establishment of the head-to-tail body axis [13].

The bidirectionality of the structural transition in developing epithelia—some are initially hexagonal and evolve into a disordered pattern whereas others undergo the disordered-hexagonal transition—supports the assertion that cell proliferation may not be an essential element of epithelial morphogenesis. Moreover, in some animals certain stages of the process depend on programmed cell death [16]. In addition, during the transition cell walls "grow and shrink" [12], which leads to rearrangement of neighbors suggesting that the tiling explores many possible configurations in a series of quasiequilibrium states.

Based on these facts, we propose an equilibrium model of polygonal tilings to explain the structure of simple columnar epithelia. We focus on assemblies of elongated cells whose energy does not depend on their shape and whose basic morphometric features are well defined. We study the entropy-maximizing structure of the model tissue by numerically exploring all possible cell arrangements and we identify two distinct phases, which are both observed in epithelia and other layered cell aggregates. With its unspecific packing nature, our model may help to elucidate the origin of certain patterns shared by many animal tissues and species.

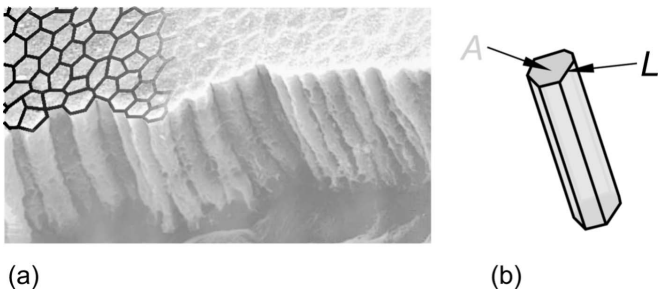

FIG. 1. The structure of simple epithelium (a) consisting of a single layer of elongated prismatic cells (SEM of mucosal epithelium in rat small intestine; image courtesy of Dr. Roger Wagner, University of Delaware) is uniquely described by their bases that form a polygonal tiling partly outlined at the apical surface. The shape of cells (b) is a prism with a base of area A and perimeter L. In our model, A and L are assumed to be fixed and identical in all cells described by base reduced area $a=4\pi A/L^2$.

 ©2009 The American Physical Society

II. MODEL AND RESULTS

A. Energy-degenerate cell shapes

For simplicity, we restrict the discussion to single-layer epithelia consisting of prismatic cells that have the same and invariable height, volume, and membrane area. In this case, the areas and the perimeters of cell polygonal bases are also fixed and identical in each cell. Base area A and perimeter L [Fig. 1(b)] can be conveniently combined into the so-called reduced area (sometimes called the shape factor [17])

$$a = \frac{4\pi A}{L^2}, \tag{1}$$

a geometric parameter that measures the inflatedness of the base contour. For isolated contours, the largest possible value of a is 1 which describes a circle, whereas in a tiling of polygons of identical areas and perimeters it cannot exceed 0.907; this corresponds to regular hexagons.

As the intralayer cell-cell adhesion between epithelial cells is very strong, an immediate consequence of the fixed cell base perimeter is that the energy of cells does not depend on the shape of the base. This remarkable property has been emphasized in the analysis of the epithelial theory based on cortex elasticity [11] but is also characteristic of a model built upon the bending elasticity of the lipid bilayer membrane. In elongated prismatic cells [Fig. 1(a)] both bending and adhesion energy are dominated by the contributions of the lateral faces. The bending energy of each cell is given by $W_b=(Kh/2)\oint C^2(s)ds$, where K is the bending constant [18] and h is cell height; the integral runs along the base contour, a planar loop of fixed length L, and $C(s)$ is the local curvature of the contour. The adhesion energy per cell is proportional to the total length of contact sections of the base contour, $W_a=-(\Gamma h/2)\Sigma_i\int_{contact} ds_i$, where Γ is the adhesion strength. At large values of Γ, one can assume that the contact sections are straight and that the noncontact sections are circular arcs of radius R whose value must be $\sqrt{K/\Gamma}$ [19]; furthermore, observations suggest that the base is convex [12,13]. Then the total energy of a cell is

$$W = \left[\frac{\pi K}{R} - \frac{\Gamma}{2}(L - 2\pi R)\right]h \tag{2}$$

irrespective of all attributes of the shape of the base—number of vertices, internal angles, and relative lengths of contact sections—so that all cells of identical and fixed base perimeter L are energy degenerate [20].

B. Theoretical tilings

Because the energy of cells is insensitive to their shape, the cross section of the model single-layer tissue includes a multitude of local packings of polygonal contours. We explored these polygonal assemblies using Monte-Carlo-type numerical simulations implemented within the SURFACE EVOLVER package [21], which proved very suitable for an efficient bookkeeping of the large number of geometric properties of the system (polygon perimeters and areas). Starting from an ordered tiling consisting of identical flattened equilateral hexagonal tiles of a given reduced area, we applied a set of transformations including random edge length change and neighbor-swapping topological T1 process [22] to find the equilibrium structure. Each transformation was followed by a relaxation of the system to fulfill the perimeter, area, and convexity constraints; through relaxation, any single transformation affects the tiling globally. We used periodic boundary conditions in a rectangle with typically 400 polygons, which is a large enough sample to avoid finite-size effects. A few 1000 steps (each step being either a random edge length change or a T1 transformation), which usually included about 1000 T1 transformations, were sufficient to equilibrate the tiling so that the relevant structural and statistical-mechanical ensemble averages did not change anymore (Fig. 2). The data presented were collected during 3000–5000 averaging steps.

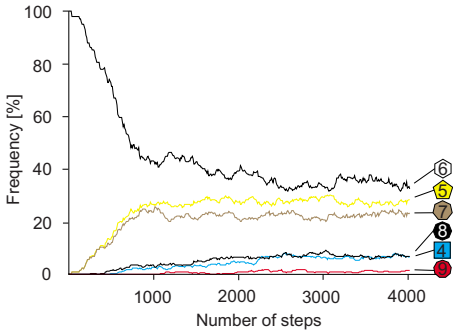

FIG. 2. (Color online) Typical evolution of the equilibrium structure of the tiling during a simulation run: the initially regular tiling consisting exclusively of hexagons with identical reduced areas a is equilibrated after a few 1000 Monte Carlo steps including a random edge length change or a T1 transformation. Upon equilibration, the frequency of hexagons decreases and the frequencies of the other polygon classes gradually increase. The data shown here correspond to an $a=0.70$ tiling (containing 400 polygons) whose equilibrium structure is disordered and includes four-, five-, six-, seven-, eight-, and nine-sided tiles.

Snapshots of thus obtained equilibrium tilings at polygon reduced areas from $a=0.74$ to $a=0.9$ shown in Fig. 3 demonstrate that depending on the value of a, the system is either ordered or disordered. For $a>0.865$, the tiling is composed exclusively of hexagons and we refer to this perfectly sixfold coordinated phase as the ordered phase. For values of a between 0.785 and 0.865, it consists of pentagons, hexagons, heptagons, and very few octagons. At $a>0.85$, pentagons and heptagons often appear in diamond-shape quadruplets produced by a single T1 edge swap on a tiling of hexagons, each quadruplet consisting of two pentagons and two heptagons. As a is decreased, the frequency of the nonhexagonal tiles increases at the expense of the hexagons. Finally, for $a<0.785$ the tiling is a strongly disordered mixture of polygons with four to nine vertices and the composition of the mixture barely depends on the reduced area across a broad range. The onset of this robust disordered structure is signaled by the appearance of quadrilaterals and the drop of frequency of pentagons and hexagons. By robust disordered phase we denote the regime where the frequencies of polygon classes are insensitive to the reduced area a. We note that the order-disorder transition and the onset of the robust

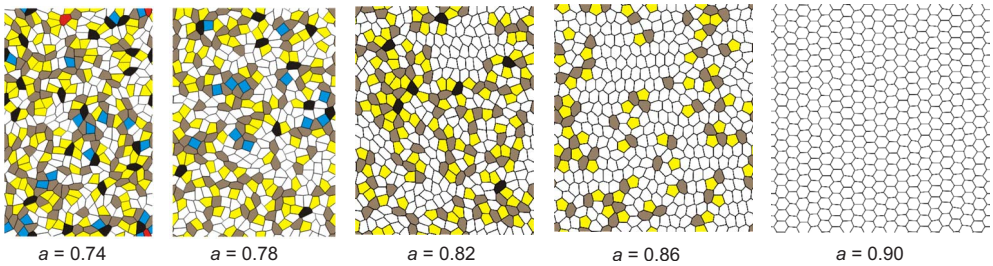

FIG. 3. (Color online) Representative snapshots of equilibrium theoretical tilings at polygon reduced areas $a=0.74$, 0.78, 0.82, 0.86, and 0.90. For values of polygon reduced area a smaller than 0.785 the tiling is disordered and includes four-, five-, six-, seven-, eight-, and nine-sided tiles whose frequencies barely depend on a; each polygon class is encoded by color or a shade of gray. Beyond $a=0.785$, the frequency of hexagons increases with a at the expense of the nonhexagonal polygons. At $a=0.865$ the order-disorder transition takes place; for $a>0.865$ all polygons in the tiling are perfectly sixfold coordinated.

disordered phase occur at the largest reduced area that can be enclosed by a pentagon ($a=0.865$) and a quadrilateral ($a=0.785$), respectively.

The composition of the tiling in terms of frequencies of polygon classes is shown in Fig. 4, which quantifies the above classification of tilings. It also emphasizes the robustness of the disordered phase for $a<0.785$ where the average frequencies of four-, five-, six-, seven-, eight-, and nine-sided polygons are 5%, 26%, 40%, 23%, 5%, and 1%, respectively; error bar magnitude is below 2%. In all tilings we explored, triangles and polygons with ten or more vertices were absent. Given that the largest reduced area that can be enclosed by a triangle is 0.605, we expect that they be present in tilings at $a<0.605$ albeit not in large numbers.

III. DISCUSSION

A. Comparison with experiments and earlier theories

These results extend the predictions of the two-parameter theory based on proliferation of adhering cells with a preferred cross-section area and a cortex elasticity [11], which gives the disordered phase and the regular crystalline version of the hexagonal phase. This theory is characterized by a rather straightforward phase diagram spanned by the cortex contractility c and line tension t, which describe the forces resulting from actin-myosin contractility and cell-cell interactions, respectively [11]. In the diagram the two phases are separated by a linear boundary described within a few percent by $c\approx -0.133t/\sqrt{A^{(0)}}$ (Fig. 5; $A^{(0)}$ is the preferred polygon area), which implies that the structure of the tiling may depend on the ratio of c and t rather than on c and t themselves. Indeed, for $t<0$ the interplay of cortex elasticity and adhesion results in a preferred polygon perimeter $L^{(0)}$ equal to $-t/2c$ such that any deviation of the perimeter from $L^{(0)}$ carries an energetic penalty [11]; this is a soft version of the fixed-perimeter constraint used in our model. Given that the theory of Ref. [11] also includes an energy term favoring a certain polygon area $A^{(0)}$, a more negative value of t/c cor-

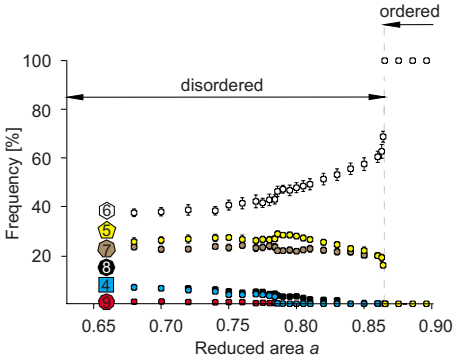

FIG. 4. (Color online) Frequencies of polygon classes as a function of reduced area: the order-disorder transition at $a=0.865$ is marked by a dramatic change in the frequencies of five-, six-, and seven-sided polygons, whereas the discontinuity of the frequencies of quadrilaterals, pentagons, hexagons, and heptagons at the onset of the robust disordered phase at $a=0.785$ is less pronounced.

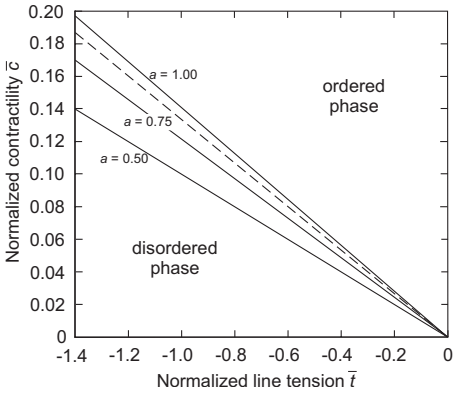

FIG. 5. Theoretical phase diagram of proliferating adhering contractile cells (adapted from Fig. 1 in Ref. [11]): depending on the effective line tension t and contractility c, the tissue can be either disordered or ordered. In the plane spanned by the normalized line tension $\bar{t}=t/\kappa[A^{(0)}]^{3/2}$ and contractility $\bar{c}=c/\kappa A^{(0)}$ (here κ denotes the elastic coefficient and $A^{(0)}$ is the preferred cell area), the order-disorder transition is described by a linear function of negative slope (dashed line). For negative values of $\bar{t}$ shown here, this model is mechanically very similar to ours except for the cell division. Each of the superimposed solid straight lines through the origin connects points in the $(\bar{c},\bar{t})$ plane that have identical values of the preferred cell reduced area $a=$const and thus identical structure; the lines are labeled by the value of a that they represent. The order-disorder transition takes place at a fixed value of $a\approx 0.89$ very close to our value of $a=0.865$ (which virtually overlaps with the dashed line).

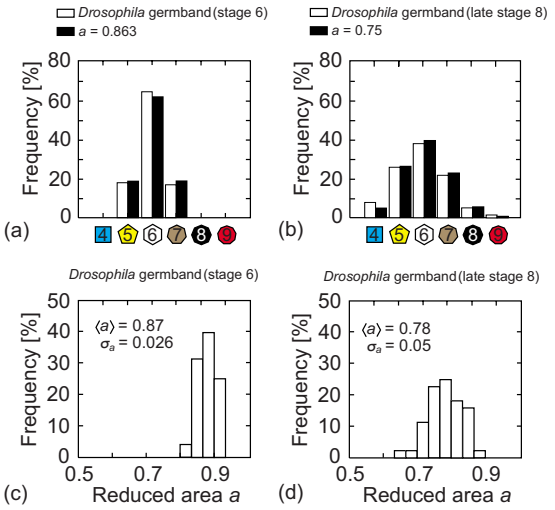

FIG. 6. (Color online) Frequencies of polygon classes in the *Drosophila* embryo germband at stage 6 (a) and late stage 8 (b): experimental data (open columns, data from Ref. [13]) agree very well with our theoretical predictions for $a=0.853$ and $a=0.75$, respectively (solid columns). From the experimental data [Figs. 2b and 2c in Ref. [13]] we also extracted the distribution of polygon reduced area in the germband shown in panels (c) and (d). The two distributions peak at the average value of $\langle a\rangle=0.87$ and $\langle a\rangle=0.78$, respectively. Although somewhat larger, these values are quite consistent with the two reduced areas of our best-fit monodisperse tilings. The dispersion of the distribution (σ_a) at stage 8 is larger than at stage 6. The bin size used here is $\Delta a=0.33$.

responds to a smaller preferred reduced area $a^{(0)}=4\pi A^{(0)}/[L^{(0)}]^2$. By combining the three parameters of this theory, we find that all along the linear boundary of the hexagonal phase the preferred polygon reduced area is $a^{(0)}\approx 0.89$ (Fig. 5), which is in excellent agreement with our hexagonal-disordered transition located at $a=0.865$. Thus we have mapped the negative-t part of the theory of Ref. [11] onto our model and we expect that the same can be done for any related theoretical framework characterized by an effective reduced area of cell cross section.

Experimental studies of epithelial geometry usually focus on the frequencies of polygon classes, the most comprehensive data sets available being those of various epithelia in *Drosophila, Hydra,* and *Xenopus* [10–13]. The phases predicted by our model agree very well with this diverse body of experimental data and generalize the results of earlier theories [10,11]. In particular, the $a=0.863$ disordered phase fits nicely with stage 6 of the *Drosophila* germband [13] and the $a=0.75$ robust disordered phase reproduces the germband at late stage 8 [Figs. 6(a) and 6(b)]. We have also analyzed the distribution of polygon reduced areas in the germband [Figs. 6(c) and 6(d)]. Although the areas and perimeters of cells in the germband are hardly monodisperse, which can be seen in the micrographs in Figs. 1a and 1b in Ref. [13], the distributions of the reduced area are surprisingly narrow. The average reduced areas at stage 6 and at late stage 8 are $\langle a\rangle=0.87$ and 0.78, respectively. These values are very close to the reduced areas of our theoretical tilings that fit the germband data best. Thus it seems that as long as the reduced area of a tiling is well defined, polydispersities of polygon areas and perimeters barely affect the topological structure of the tiling reflected in the frequencies of polygon classes. We note that the dispersion of the distribution of polygon reduced areas is larger in the more disordered tiling; it appears that in real tilings, there exists a negative correlation between the dispersion and the average value of polygon reduced area.

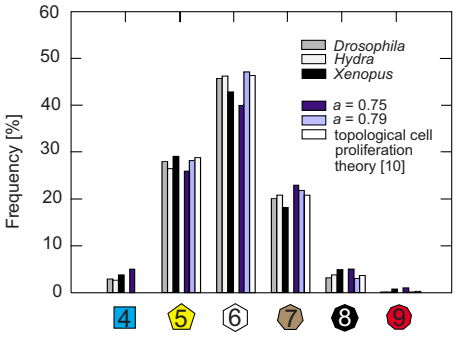

FIG. 7. (Color online) Structure of *Drosophila* wing disk, *Hydra* tail epidermis, and *Xenopus* epidermis in terms of frequencies of polygon classes (data from Ref. [10]). The three sets of experimental data agree nicely with the theory proposed in Ref. [10]. However, they are equally well described by our $a=0.79$ tiling with the polygon class frequencies virtually identical to that of Ref. [10]. The $a=0.75$ tiling reproduces the observed frequency of quadrilaterals better.

Further support for our model is found in the skewed polygon distributions in *Drosophila* wing disk as well as in *Hydra* epidermis and *Xenopus* tail epidermis [10], which are very similar to each other [10] (Fig. 7). The structure of these tissues agrees well with the single set of polygon frequencies predicted by the purely topological theory of cell proliferation [10] although the latter is devoid of quadrilaterals, which constitute about 3% of all polygons in the tissues in question. For $a\approx 0.79$, our model produces a distribution of polygon classes nearly identical to that of the theory proposed in Ref. [10], thereby providing an equally viable explanation of the experimental data. In addition, our $a=0.75$ tiling (also shown in Fig. 7) reproduces the observed frequencies of quadrilaterals much better although the agreement of the frequencies of other polygon classes is a bit worse.

Ample insight into the continuity of the order-disorder transition in polygonal tilings is provided by a study of the *Drosophila* wing epithelium [12], which includes a sequence of patterns consisting exclusively of pentagons, hexagons, and heptagons. Yet the observed tilings are quantitatively less consistent with ours, primarily because of the large frequency of pentagons. It is likely that better agreement can be achieved with a refined version of our model which would include a certain area and perimeter polydispersity characteristic of real tissues. We can conclude that the predictions of the proposed equilibrium model compare with experiments at least as well as those of the two earlier theories, which rely on cell division [10,11]. In our view, cell proliferation is of secondary importance for the structure of epithelia: the dynamics associated with cell division merely provides a way

to sample the possible states of the tissue which, if unbiased, leads to the entropy-maximizing configuration.

B. Tile-tile correlations

We also looked into structural features other than polygon frequencies. A well-established general empirical relationship describing two-polygon correlations known as the Aboav-Weaire law [22] says that in disordered cellular systems the average sum of the number of sides of nearest neighbors of an n-sided polygon, $nm(n)$, is a linear function of n:

$$nm(n) = (6 - f)n + 6f + \mu_2, \tag{3}$$

where $f \sim 1$ and $\mu_2 = \Sigma_n (n - \langle n \rangle)^2 P_n$ is the second moment of the distribution of polygon classes P_n; $\langle n \rangle$ is the average number of vertices of polygons in the tiling. We computed $nm(n)$ of the strongly disordered tilings and found that the Aboav-Weaire law is obeyed perfectly at all values of a. In the strongly disordered phase, $f \approx 1.1$ and $\mu_2 \approx 0.95$ almost irrespective of a. These rather small values of f and μ_2 reflect the considerable regularity of our tilings where all polygons have identical areas and perimeters; the fixed-area and fixed-perimeter constraints apparently disfavor tilings with a broad distribution of polygon classes. As tile reduced area is increased beyond the onset of the robust disordered phase, f and μ_2 gradually decrease and in the hexagonal phase with perfect sixfold coordination, they both vanish.

Another type of correlations studied were those characteristic of liquid-crystalline order. As the polygons assume an increasingly more elongated shape as a is decreased, one would expect that at small enough reduced areas the nearby polygons be aligned. But we find that the global nematic order parameter is 0 across the whole range of a discussed here. The most likely reason for the absence of the orientational order is the requirement that the tiling be gapless, which apparently introduces enough mixed contacts between the long and the short sides of neighboring tiles to suppress the alignment of their long axes.

C. Statistical mechanics of tilings

Because the isoperimetric polygon shapes are energy degenerate, the equilibrium structure of the tiling is determined by the maximum entropy principle [23,24], which must be applied within a consistent statistical-mechanical framework. Such a theory has been elaborated by Edwards and coworkers within the context of granular materials as manifestly nonthermal ensembles [25] but it also covers cellular systems such as foams and tissues [26]. In this formalism, each polygon is divided into quadrons—quadrilaterals defined by a vertex, the midpoints of edges that meet at it, and the polygon centroid [Fig. 8(b)]. Given that the number of independent degrees of freedom matches the number of quadrons and that the sum of quadron areas is the total tiling area, which is the 2D cellular analog of the conventional Hamiltonian, one is led to infer that the quadrons are the elementary quasiparticles of a tiling [26,27], their areas $a_1, a_2, \ldots$ being the independent degrees of freedom.

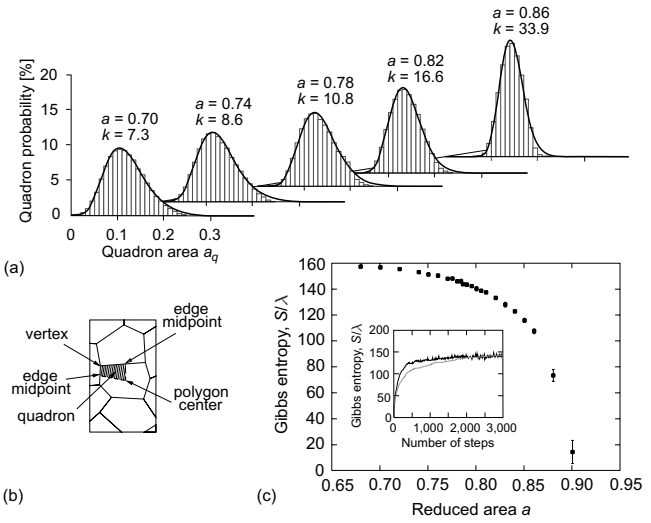

FIG. 8. Statistical-mechanical properties of tilings. (a) Quadron PDF for representative polygon reduced areas corresponding to disordered tilings. The PDFs are increasingly more narrow and less right-skewed as a is increased and agree with the gamma distribution (solid curves) except for the right tail, which is suppressed by the fixed-area constraint that each polygon must satisfy. The gamma distribution shape parameter k, which increases with polygon reduced area a, is an estimate of the number of quadrons in correlation clusters. (b) Quadrons, the independent degrees of freedom in a two-dimensional (2D) cellular network, are convex quadrilaterals spanned by a vertex, midpoints of adjacent edges, and polygon centroid. (c) The Gibbs entropy of the equilibrium tiling is a decreasing function of a and bears no obvious signature of the onset of the robust disordered phase and the disordered-hexagonal transition, suggesting that they are continuous. Inset: at the beginning of the simulation run, the entropy increases until the initial hexagonal state reaches equilibrium after a few 1000 steps. Compared here are the entropies of an $a=0.81$ tiling in a box containing 400 and 1600 polygons (black and gray curve, respectively) to show that finite-size effects are negligible in a system of ~ 100 tiles.

The statistical-mechanical state of a tiling is encoded in the density of quadron areas $\Theta(a_1, a_2, \ldots)$. Were the quadrons uncoupled, $\Theta(a_1, a_2, \ldots)$ would be a product of identical single-quadron factors: $\Theta(a_1, a_2, \ldots) = p(a_1)p(a_2)\ldots$ But this is not the case: quadrons must tile the plane and those belonging to the same polygon must satisfy the fixed-area and fixed-perimeter constraints, which makes them strongly correlated. As a result, a detailed analysis of their entropy is fairly complicated. Here we estimate it using Gibbs formula $S = -\lambda \int \tilde{p}(a_q) \ln \tilde{p}(a_q) da_q$, where $\tilde{p}(a_q)$ is the averaged projection of $\Theta(a_1, a_2, \ldots)$ onto the single-quadron phase spaces [shortly the probability density function (PDF)] and λ is the analog of the Boltzmann constant.

The PDFs of our tilings [shown in Fig. 8(a)] are right-skewed and the location of their peak increases with polygon reduced area a; the distribution is narrow at large values of a but broadens as a is decreased. Virtually all details of the PDFs are described by the gamma distribution [28,29]:

$$p(k,\langle a_q\rangle,a_q) = \frac{k}{\langle a_q\rangle\Gamma(k)}\left(\frac{ka_q}{\langle a_q\rangle}\right)^{k-1}\exp\left(-\frac{ka_q}{\langle a_q\rangle}\right), \qquad (4)$$

where a_q is the quadron area and $\langle a_q\rangle$ is its ensemble average, k is the shape parameter, and $\Gamma(k)$ is the gamma function. The fit is almost perfect at all values of a, the only systematic discrepancy being the large-a_q tail, which is suppressed by the fixed-area constraint imposed on each polygon. The shape parameter depends strongly on polygon reduced area increasing from $k\approx 7.3$ at $a=0.70$ to $k\approx 76.4$ at $a=0.88$. The PDFs disclose valuable insight into the correlations within the tiling. Recall that for integer values of k, $p(k,\langle a_q\rangle,a_q)$ is the aggregate distribution of the sum of k exponentially distributed independent random variables of identical means [28]—in our case, the areas of quadrons, which obey the Maxwell-Boltzmann distribution [27]. If we imagine that the tiling consists of quadron clusters just big enough to satisfy both local and global constraints, then these clusters reproduce all the statistics of an infinite system including the long-range features. Thus the shape parameter k extracted from the PDFs can be interpreted as the number of quadrons in these clusters and the cluster radius, $\sqrt{k\langle a_q\rangle/\pi}$, measures the range of correlations. In the strongly disordered phase with $a=0.70$ where $k\approx 7.3$, each quadron is strongly correlated only with its nearest and next-nearest neighbors (consistent with the absence of long-range nematic order mentioned above), whereas in the hexagonal phase at $a=0.88$ the clusters include about 76.4 quadrons, i.e., ≈ 13 tiles.

Figure 8 also shows the Gibbs entropy of the tilings as a function of polygon reduced area. The entropy was calculated by approximating the integral by a sum over all bins of the histograms of the PDFs, $S=-\lambda\Sigma_i p_i \ln p_i$. As expected, entropy is a decreasing function of a. However, it bears no clear signature of the onset of robust disordered phase and the disordered-hexagonal phase transitions, which agrees with the continuous dependence of the structural features of tilings on polygon reduced area and implies that the transitions are second order. This is plausible yet we cannot rule out the possibility that a more refined evaluation of entropy that includes the quadron-quadron correlations in full may depart somewhat from these results and we will address this point in the future.

IV. CONCLUSIONS

The good agreement of our theoretical entropy-maximizing tilings with those observed in simple epithelia suggests that these tissues develop by passing through a sequence of quasiequilibrium states. This view represents an alternative to theories of epithelial structure based on cell proliferation [10,11] and it generalizes their findings although it relies on fewer assumptions and parameters. Another important feature of the proposed model is that it singles out the tile reduced area as the only quantity that controls the structure of the tilings. Given that the reduced area is a purely geometric and aggregate parameter of the underlying biomechanics, the various physiologically relevant physical descriptions of epithelia should all produce the same structure as long as they are characterized by identical effective cell reduced area. Thus the model presented here can be regarded as a step toward the mechanisms of universality that is observed in two-dimensional cellular structures.

ACKNOWLEDGMENTS

We are indebted to R. Wagner for the micrograph shown in Fig. 1 and to S. El Shawish for providing us with the data presented in Figs. 6(c) and 6(d). We thank J. Dobnikar, G. Kahl, R. D. Kamien, M. Miettinen, R. Podgornik, A. Šiber, E. Trizac, and G. Vidmar for stimulating discussions. This work was supported by Slovenian Research Agency through Grant No. P1-0055.

[1] D. W. Thompson, *On Growth and Form*, 2nd ed. (Cambridge University Press, Cambridge, 1942).
[2] T. Hayashi and R. W. Carthew, Nature (London) **431**, 647 (2004).
[3] J. A. Glazier and F. Graner, Phys. Rev. E **47**, 2128 (1993).
[4] J. Käfer, T. Hayashi, A. F. M. Marée, R. W. Carthew, and F. Graner, Proc. Natl. Acad. Sci. U.S.A. **104**, 18549 (2007).
[5] R. Keller, L. A. Davidson, and D. R. Shook, Differentiation **71**, 171 (2003).
[6] J. D. Axelrod, Cell **126**, 643 (2006).
[7] D. J. Montell, Science **322**, 1502 (2008).
[8] N. J. Savill and P. Hogeweg, J. Theor. Biol. **184**, 229 (1997).
[9] C. M. Nelson, R. P. Jean, J. L. Tan, W. F. Liu, N. J. Sniadecki, A. A. Spector, and C. S. Chen, Proc. Natl. Acad. Sci. U.S.A. **102**, 11594 (2005).
[10] M. C. Gibson, A. B. Patel, R. Nagpal, and N. Perrimon, Nature (London) **442**, 1038 (2006).
[11] R. Farhadifar, J. C. Röper, B. Algouy, S. Eaton, and F. Jülicher, Curr. Biol. **17**, 2095 (2007).
[12] A. K. Classen, K. I. Anderson, E. Marois, and S. Eaton, Dev. Cell **9**, 805 (2005).
[13] J. A. Zallen and R. Zallen, J. Phys.: Condens. Matter **16**, S5073 (2004).
[14] D. D. O'Keefe, D. A. Prober, P. S. Moyle, W. L. Rickoll, and B. A. Edgar, Dev. Cell **311**, 25 (2007).
[15] R. Wootton, Annu. Rev. Entomol. **37**, 113 (1992).
[16] Y. Toyama, X. G. Peralta, A. R. Wells, D. P. Kiehart, and G. S. Edwards, Science **321**, 1683 (2008).
[17] P. P. Lewicki and R. Porzecka-Pawlak, J. Food Eng. **66**, 43 (2005).
[18] U. Seifert, Adv. Phys. **46**, 13 (1997).
[19] J. Derganc, B. Božič, S. Svetina, and B. Žekš, Biophys. J. **84**, 1486 (2003).
[20] In the moderate adhesion regime, the force balance at vertices would somewhat restrict the base geometry [P. Ziherl and S. Svetina, Soft Matter **4**, 1937 (2008)] but in the $\Gamma\rightarrow\infty$ limit

that we are interested in, $R=\sqrt{K/\Gamma}\to 0$ and the total energy reduces to $W=-\Gamma Lh/2$. As L and h are fixed, so is the total energy regardless of the shape of the base.

[21] K. Brakke, Exp. Math. **1**, 141 (1992); SURFACE EVOLVER is available at http://www.susqu.edu/facstaff/b/brakke/evolver/evolver.html

[22] D. Weaire and N. Rivier, Contemp. Phys. **25**, 59 (1984).

[23] M. A. Peshkin, K. J. Strandburg, and N. Rivier, Phys. Rev. Lett. **67**, 1803 (1991).

[24] J. R. Iglesias and R. M. C. de Almeida, Phys. Rev. A **43**, 2763 (1991).

[25] S. F. Edwards and R. S. B. Oakeshot, Physica A **157**, 1080 (1989).

[26] R. Blumenfeld and S. F. Edwards, Phys. Rev. Lett. **90**, 114303 (2003).

[27] R. Blumenfeld and S. F. Edwards, Eur. Phys. J. E **19**, 23 (2006).

[28] T. Aste, T. Di Matteo, M. Saadatfar, T. J. Senden, M. Schröter, and H. L. Swinney, EPL **79**, 24003 (2007).

[29] G. Frenkel, R. Blumenfeld, Z. Grof, and P. R. King, Phys. Rev. E **77**, 041304 (2008).